DAΦNE INJECTION KICKER: ELECTROMAGNETIC ANALYSIS OF TRAPPED MODES AND DAMPING ANTENNA DESIGN

D. Alesini, S. De Simone, A. Gallo, A. Ghigo, F. Marcellini
LNF-INFN, Frascati, Italy

Abstract

During the commissioning of the Frascati Φ-Factory DAΦNE, vertical and longitudinal multibunch coupled bunch oscillations have been observed. Modal analysis and measurement of the instability thresholds as a function of local orbit bumps have shown that, with high probability, the coupled bunch oscillations can be attributed to the beam interaction with parasitic resonant modes trapped in the injection kickers. By means of theoretical models and computer simulations (based on HFSS code by HP) an electromagnetic characterization of the kickers HOMs has been carried out and the obtained results have been compared with the impedance measurements made on a prototype. The study and design of a damping antenna coupled with the structure resonant modes is described. Measurements on a prototype equipped with two antennas confirm the effectiveness of the proposed solution to strongly reduce the kicker longitudinal and vertical coupling impedances, i.e. to eliminate the instability sources.

INTRODUCTION

Three injection kickers are installed on each DAΦNE main ring in order to inject the bunches coming from the transfer lines on the correct orbit without significant loss of the already stored beam. The horizontal kick is obtained by a vertical magnetic field produced by the current flowing in two parallel coils and produced by the discharge of a capacitor connected to the coils and, on the other side, to the pulse generator circuit [1,2] as shown schematically in Fig. 1 (the kickers are the black blocks).

In this paper we describe the electromagnetic analysis of the trapped e.m. modes in the structure. The analysis is based on transmission line models (§ 1.1) and on computer simulations with HFSS (§ 1.2) (computer code based on FEM [9]) and it allows us to isolate the different resonant modes that interact longitudinally or transversely with the beam. We compare also the theoretical results with the impedance measurements (§ 2.1-2-3). To measure the impedance we utilized the Sands and Rees method [3-8].

We describe, then, the design of a damping antenna coupled with the resonant modes in the structure to reduce the kicker impedance. The analysis of the antenna frequency response is based on transmission line models (§ 3.1) and HFSS simulations (§ 3.2).

Finally we compare the theoretical results with measurements made on a prototype equipped with two antennas (§ 4.1-2-3).

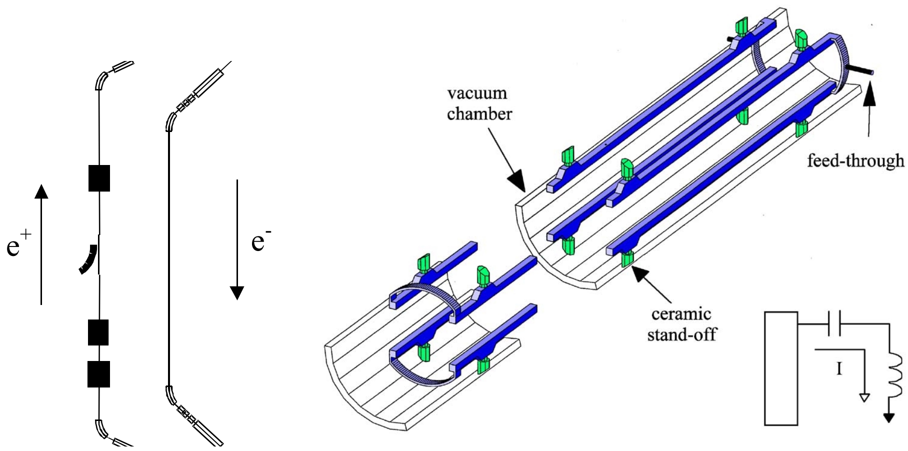

Figure 1: layout of the machine injection section and kicker schematic view.

1 ELECTROMAGNETIC ANALYSIS OF THE KICKER TRAPPED MODES

1.1 Transmission line model

The model adopted to describe the resonant trapped modes in the kickers is shown in Figure 2.

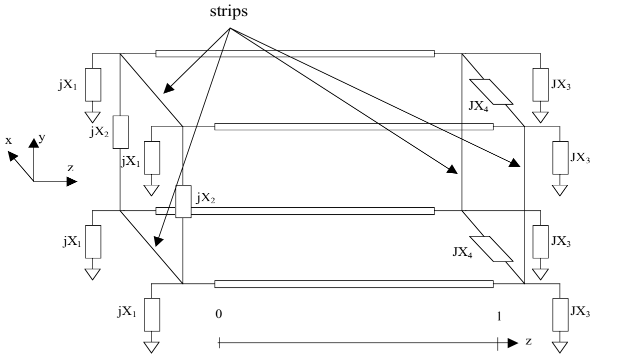

Figure 2: multiconductor transmission line model of the kicker.

We can consider the kicker like a multiconductor transmission line terminated on reactive loads that model the discontinuity between the coils and the vacuum chamber.

In this model we neglect:

a) the presence of dielectric stand-offs;

b) the presence of the external pulse generation system.

In the model introduced in Figure 2 we could consider the stand-offs as localized impedances along the transmission lines. They will shift the resonance frequencies of the structure and perturb locally the e.m. fields. From dedicated simulations and measurements we have concluded that the perturbation is negligible.

To take into account the presence of the external circuit we should introduce two extra loads (as shown in Figure 3) whose frequency response is, unfortunately, very difficult to measure or to simulate. We will study, hence, the resonances of the structure decoupled from the external circuit and discuss later the effect of the external circuit and the limits of our approximations.

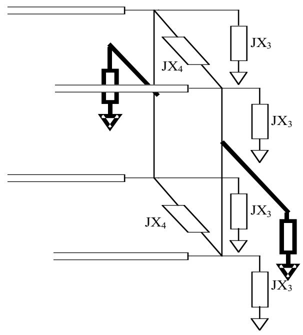

Figure 3: loads representing the external circuit in the transmission line model.

If we choose a suitable set of independent TEM modes with the same symmetry of the kicker in the xy plane, we can reduce the study of the resonances of the complete multiconductor transmission line structure to the study of the resonances of four simple decoupled transmission lines (Figure 4). We will classify these independent resonant modes with the labels HH EH HE EE because there are two planes of symmetry that are electric or magnetic.

The modal analysis is helpful in understanding which trapped modes interact with the beam. We note that only the EH mode can interact with the beam vertically because it has a vertical component of the electric field along the structure and similarly the mode HE interacts with the beam horizontally.

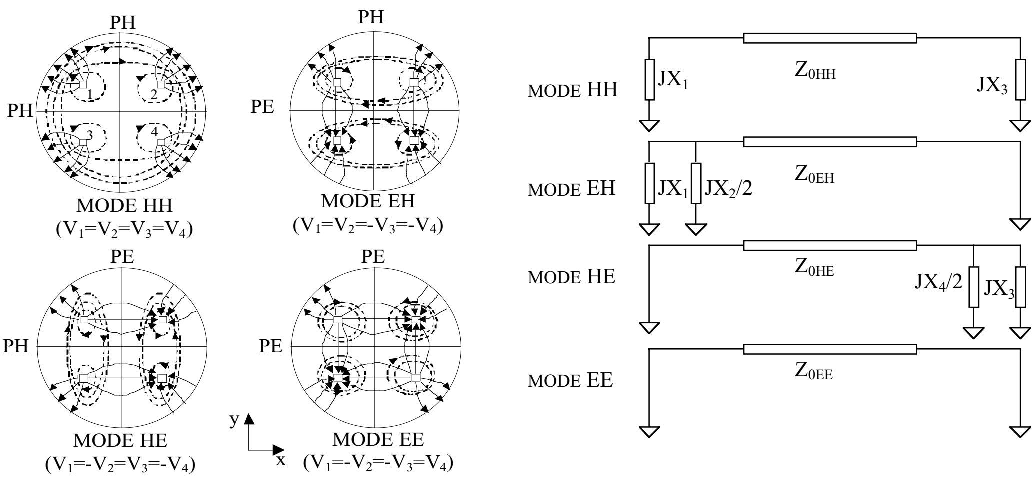

Figure 4: set of the TEM independent modes and corresponding two-conductor transmission lines.

The mode HH is the only one that can interact longitudinally with the beam because it has a longitudinal component of the electric field while the mode EE doesn't interact with the beam.

Because some vertical and longitudinal instabilities have been observed in the DAΦNE beam, we are mostly interested in the EH and HH modes.

By approximating the loads of the multiconductor transmission line with some simple capacitors, it is also possible to calculate the resonant frequencies (Table 1) and the distribution of voltage and current along the structure for each resonant mode, that corresponds to the distribution of the transverse electric and magnetic fields along the structure (Figure 5).

Table 1: resonant frequencies (in MHz) obtained by the transmission line model.

MODE HH	**MODE EH**	**MODE HE**	**MODE EE**
143.23	73.73	73.25	149.70
286.52	221.21	219.76	299.40
429.93	368.69	366.31	449.10
573.51	516.20	512.92	598.80
717.29	663.75	659.63	748.50
861.31	811.33	806.44	898.20
1005.60	958.96	953.38	1047.90
1150.16	1106.64	1100.45	1197.60
1295.01	1254.38	1247.65	1347.31
1440.14	1402.18	1395.00	1497.01

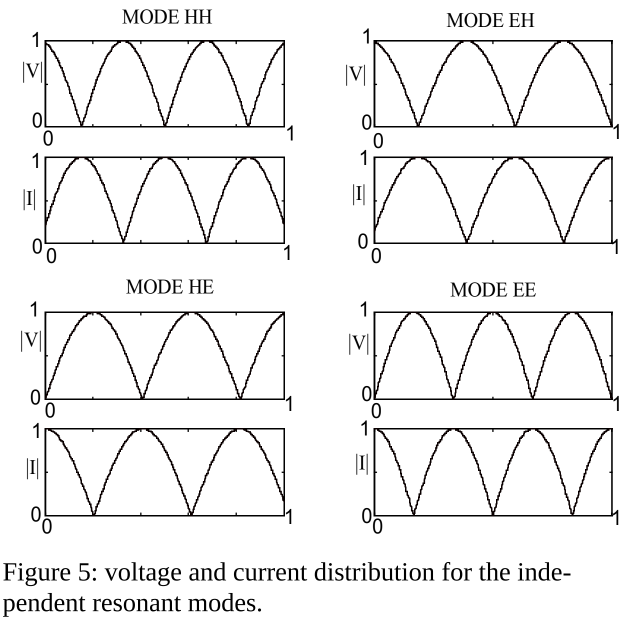

Figure 5: voltage and current distribution for the independent resonant modes.

1.2 HFSS simulations

By HFSS simulation runs of the structure of Figure 6 with the proper boundary conditions it is possible to calculate:

a) the distribution of the transverse electric and magnetic fields along the structure. Figure 7 shows the distribution of the Electric and Magnetic transverse fields along the structure. We recognize the behavior of the voltage and current in the transmission line model (Figure 5) and the characteristic capacitor effect under the coil connession strip;

a) the behavior of the longitudinal component of the electric field along the structure used for the calculation of the coupling impedances (Figure 8);

a) the behavior of the electric or magnetic field at any section of the structure.

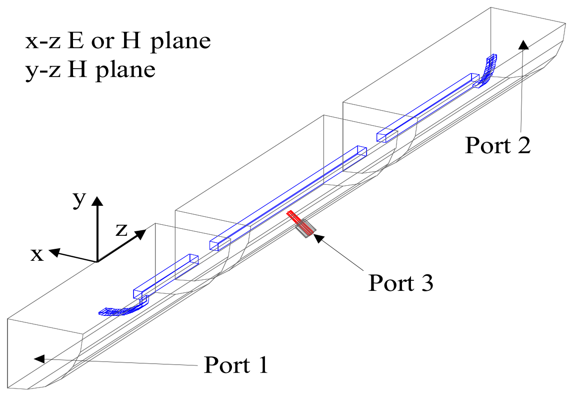

Figure 6: simulated structure by HFSS.

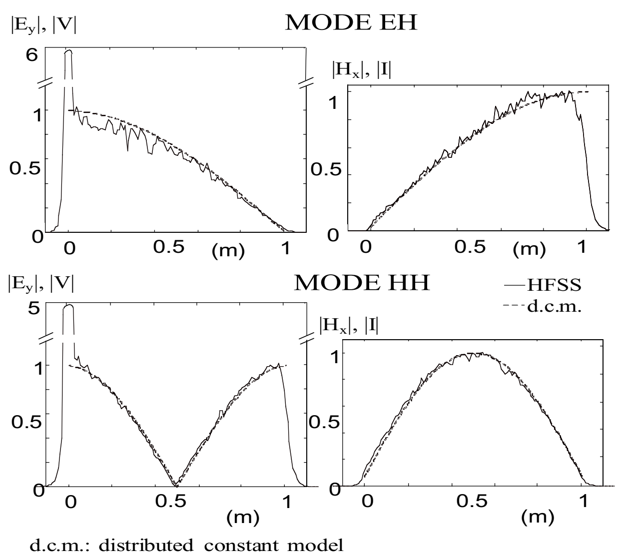

Figure 7: E_y and H_x components along the structure obtained by HFSS.

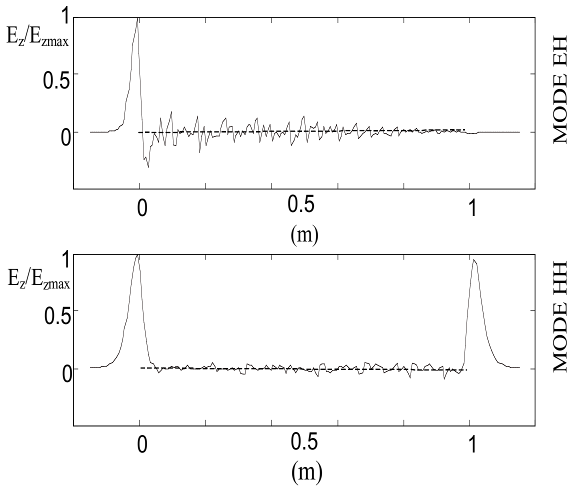

Figure 8: Re(E_z) component along the structure obtained by HFSS.

In Tables 2-3 we summarize the calculated shunt resistances and quality factors for each resonance.

We observe that in the longitudinal case (mode HH) there are two peaks of the longitudinal electric field corresponding to the two discontinuities. Since to the first-order the two kicks cancel out, the longitudinal impedance is essentially due to the peak unbalance, and therefore the computed value is greatly affect by the precision of the computer code. It means that a little error in the resonant frequency calculation or in the configuration of the field can give a strong variation of the calculated shunt resistances. For example, if we consider an error of ±1% in frequency, we obtain a large variation in the shunt resistance calculation as shown in Figure 9 (a).

The vertical case, instead, where there is only one peak in the longitudinal electric field, is less critical with respect to the precision of the code (Figure 9 (b)).

Table 2: results obtained by HFSS (longitudinal case).

Longitudinal case (HH)								
Res. Freq. (t.l.m.) [MHz]	Res. Freq. (HFSS) [MHz]	Q_0	R_{s0} (Ω)			R_{s0}/Q_0 ($\times 10^{-2}$ Ω)		
				- 1 % freq. variat.	+ 1 % freq. variat.		- 1 % freq. variat.	+ 1 % freq. variat.
143.23	**139.1**	**1009**	**142**	228	77	**14.07**	22.60	7.63
286.52	**278.3**	**1346**	**338**	551	176	**25.11**	40.94	13.08
429.93	**418.4**	**1724**	**585**	966	297	**33.93**	56.03	17.23
573.51	**558.6**	**1567**	**735**	1260	347	**46.90**	80.41	22.14
717.29	**698.8**	**1806**	**732**	1269	338	**40.53**	70.27	18.72
861.31	**838.4**	**2520**	**1171**	2003	550	**46.47**	79.48	21.83
1005.60	**979.3**	**3124**	**1459**	2489	685	**46.70**	79.67	21.93
1150.16	**1123.0**	**2339**	**835**	1586	312	**35.70**	67.81	13.34
1295.01	**1266.4**	**2745**	**966**	1880	338	**35.19**	68.49	12.31
1440.14	**1406.5**	**3386**	**1099**	2172	369	**32.46**	64.15	10.90
1585.54	**1546.6**	**2920**	**924**	1842	297	**31.64**	63.08	10.17
1731.22	**1690.6**	**3803**	**1040**	2131	322	**27.35**	56.03	8.47
1877.15	**1834.3**	**3801**	**995**	2132	267	**26.18**	56.09	7.02
2023.33	**1972.5**	**3002**	**707**	1557	168	**23.55**	51.87	5.60
2169.73	**2111.3**	**4611**	**1173**	2377	342	**25.44**	51.55	7.42
2316.35	**2258.9**	**4587**	**874**	1924	228	**19.05**	41.94	4.97
2463.17	**2400.2**	**4389**	**785**	1848	150	**17.89**	42.11	3.42

t.l.m. = transmission line model

Table 3: results obtained by HFSS (transverse case).

Transverse case (EH)											
Res. Freq. (t.l.m.) [MHz]	Res. Freq. (HFSS) [MHz]	Q_0	R_{s1} (Ω)			$R_{s\perp}$ (KΩ/m)			R_{s1}/Q_0 ($\times 10^{-1}\ \Omega$)		
				- 1 % freq. variat.	+ 1 % freq. variat.		- 1 % freq. variat.	+ 1 % freq. variat.		- 1% freq. var.	+1% freq var.
73.73	**70.9**	**750**	**1876**	1877	1875	**8080**	8084	8076	**25.01**	25.03	25.00
221.21	**212.8**	**1670**	**1243**	1250	1235	**1782.7**	1812.1	1753.9	**7.44**	7.49	7.40
368.69	**355.1**	**1693**	**932**	950	914	**801.34**	808.89	793.78	**5.51**	5.61	5.40
516.20	**498.0**	**1722**	**652**	677	627	**399.65**	411.29	388.07	**3.79**	3.93	3.64
663.75	**637.6**	**2920**	**813**	868	760	**389.23**	411.47	367.43	**2.78**	2.97	2.60
811.33	**780.1**	**2772**	**618**	682	557	**241.90**	264.25	220.26	**2.23**	2.46	2.01
958.96	**922.9**	**3581**	**778**	895	668	**257.49**	293.35	223.20	**2.17**	2.50	1.87
1106.64	**1063.0**	**3872**	**577**	703	462	**165.76**	199.86	134.15	**1.49**	1.82	1.19
1254.38	**1205.3**	**3189**	**419**	545	307	**106.12**	136.63	78.51	**1.31**	1.71	0.96
1402.18	**1345.5**	**4500**	**491**	690	323	**111.44**	155.07	74.12	**1.09**	1.53	0.72
1550.05	**1482.6**	**5213**	**391**	632	203	**80.47**	128.86	42.18	**0.75**	1.21	0.39
1697.98	**1622.7**	**4444**	**272**	502	104	**51.22**	93.44	19.76	**0.61**	1.13	0.23
1845.98	**1762.8**	**5577**	**267**	574	69	**46.30**	98.41	11.99	**0.48**	1.03	0.12
1995.04	**1889.7**	**4838**	**104**	321	9	**16.74**	51.32	1.55	**0.21**	0.66	0.02

t.l.m. = transmission line model

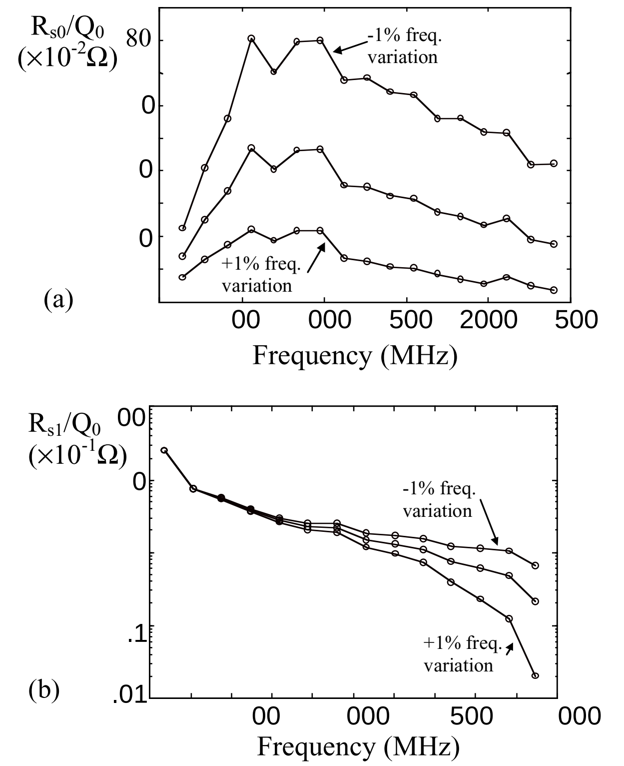

Figure 9: R/Q in the longitudinal (a) and transverse (b) case for ±1% resonant frequency variation.

2 MEASUREMENTS ON THE PROTOTYPE

2.1 Wire measurements

The results of the wire measurements (Sands and Rees method) made on a prototype are shown in Figure 10.

Each peak corresponds to a resonance in the structure. Figure 11 shows the results of the R/Q measurements in the longitudinal and vertical case compared to the computer simulations. To realistically compare the measurements and simulations in the longitudinal case, one has to consider, for the simulation results, the range shown in Figure 11 (a). In fact, by simulation on simple test structures, we concluded that the code underestimates the frequency of the resonant modes by 1-2% typically.

In the vertical case, instead, there is very good agreement between simulations and measurements.

2.2 Q measurements

To check the reliability of the wire measurements we made Q measurements by exciting the resonances in the structure with a little probe. Table 4 shows the results of the wire measurements compared to the Q ones. We can observe the good agreement between the results.

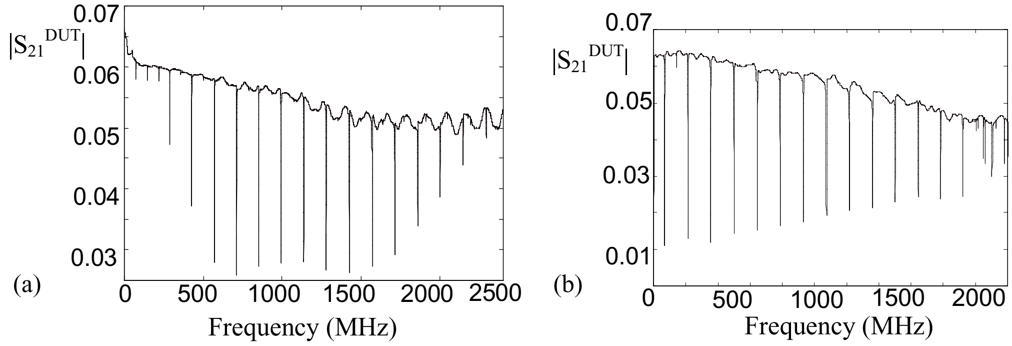

Figure 10: $|S_{21}|^{DUT}$ obtained by the measure of the longitudinal (a) and vertical (b) impedance.

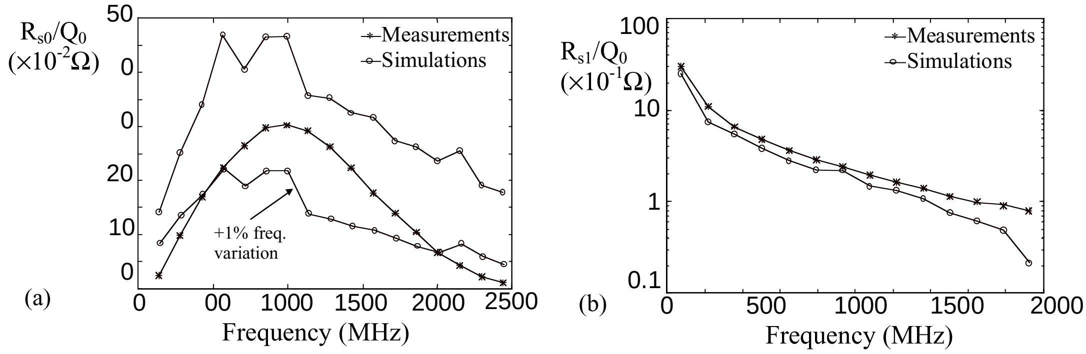

Figure 11: R/Q obtained by the wire measurements and the simulation in the longitudinal (a) and vertical (b) case.

Table 4: Q measurements compared with wire measurements.

LONGITUDINAL CASE

	Q MEASUREMENTS		*WIRE MEASUREMENTS*	
	Res. freq. (MHz)	**Q_0**	**Res. freq. (MHz)**	**Q_0**
1	142.2	861	142.4	854
2	282.5	1293	283.3	1113
3	424.9	1896	426.1	1579
4	567.4	2123	568.9	1886
5	709.1	1980	710.8	1776
6	849.9	1441	851.7	1509
7	990.8	1209	992.8	1351
8	1133.4	1338	1135.2	1387
9	1277.7	1684	1279.5	1572
10	1423.5	2107	1425.2	1832
11	1569.1	2147	1570.7	1946
12	1713.6	2065	1715.1	1915
13	1857.2	1938	1858.8	1839
14	2001.1	1891	2002.6	1800

TRANSVERSE CASE

	Q MEASUREMENTS		*WIRE MEASUREMENTS*	
	Res. freq. (MHz)	**Q_0**	**Res. freq. (MHz)**	**Q_0**
1	71.3	641	71.7	597
2	215.5	937	215.2	765
3	359.2	1172	358.6	1110
4	503.0	1288	502.2	1279
5	646.8	1418	645.8	1392
6	790.6	1558	789.4	1516
7	934.2	1601	932.7	1571
8	1077.5	1581	1075.8	1621
9	1215.6	1510	1218.7	1667
10	1363.4	1750	1361.4	1664
11	1505.6	1737	1503.8	1739
12	1647.2	1795	1645.7	1858
13	1787.3	1802	1786.0	1826
14	1922.7	1381	1921.8	1824

2.3 Measurements including pulse generation system

In our treatment we assumed the kicker as decoupled from the external circuit. The pulse generation system, in principle, does not influence the EH mode because, in order to consider the dipole modes, one has to cut the kicker horizontally (xz plane) with an electric plane, and the loads that model the external circuit are short circuited by the electric plane itself.

In the longitudinal and horizontal cases, on the contrary, the situation is more complicate because the loads that model the external circuit are cut by a magnetic plane. The configuration of the resonant modes is more complicate and, in general, we will have an hybrid resonant mode (not a pure HH mode anymore).

In conclusion the external circuit is not coupled to the EH mode (vertical impedance), and our approach in this case is correct.

In the longitudinal case, instead, there is coupling to the external circuit and our approach is less rigorous than in the vertical case.

To confirm this conclusion we have made vertical and horizontal transverse impedance measurement with and without the external circuit (Figure 12).

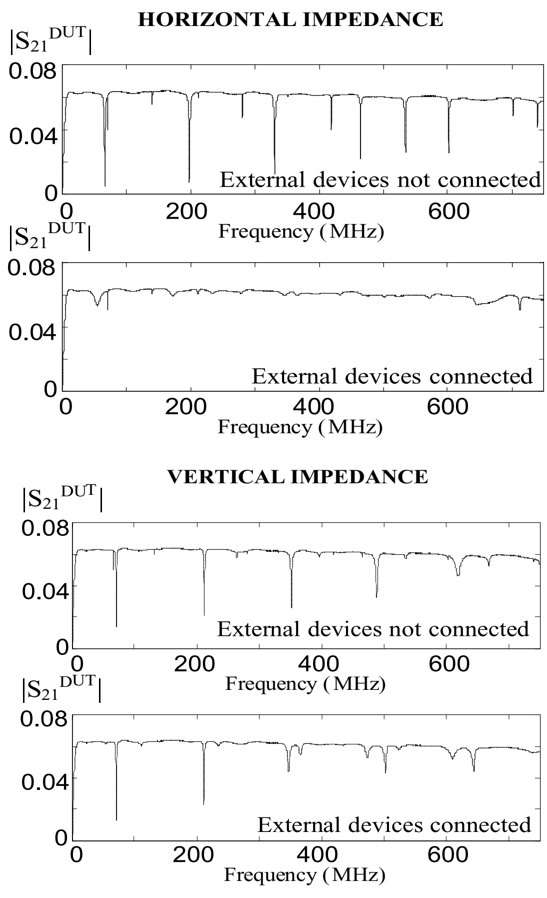

Figure 12: $|S_{21}|^{DUT}$ wire measurements with and without the external circuit.

We noticed that in the vertical case there are no differences between the two cases, while in the horizontal one, because of the coupling between the modes in the structure and the external circuit, the difference is large.

3 ANTENNA DESIGN

We can consider two different types of antenna: antennas coupled electrically and antennas coupled magnetically with the e.m. fields in the structure.

With simple probes or loops we can obtain, however, only low values of the coupling factor β (<1).

We proposed the solution shown in Figure 13. It is an antenna coupled electrically with the resonant field and positioned under the connecting strips of the coils. The antenna is made by a plate connected with the output coaxial line by a 50 Ohm strip. This connection strip is necessary to place the vacuum feedthrough in a mechanically accessible point.

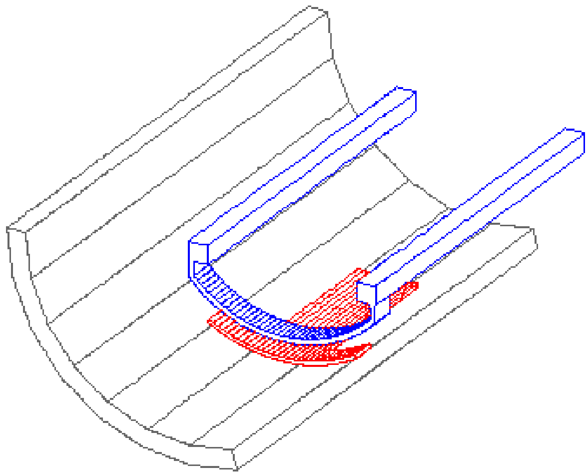

Figure 13: proposed solution for the damping antenna.

3.1 Transmission line model of the antenna

The antenna equivalent circuit is shown in Figure 14. In it:

a) C_1 and C_2 model the capacities between the strip of the coil and the plate of the antenna and between the plate and the vacuum chamber;

b) the line L_0 models the connection strip between the plate and feedthrough;

c) the line L_1 models the matched output coaxial line;

d) the line L_2 models the transmission line represented by the coil;

e) the reactance jB models the fringing effects at the junction strip-coaxial line.

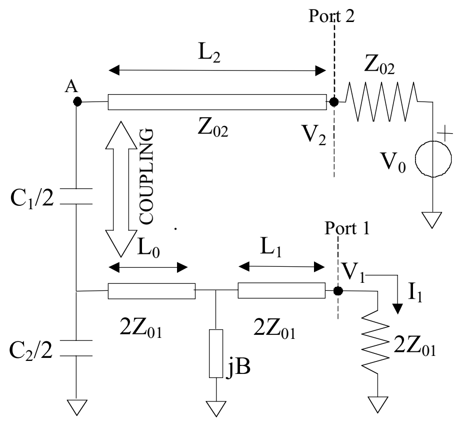

Figure 14: equivalent circuit of the antenna.

With this simple model it is possible to describe the variation of the antenna coupling with its geometrical dimensions.

Figure 15 shows the $|S_{21}|$ scattering parameter in the circuit of Figure 14 versus the plate dimension. This scattering parameter is directly correlated to the external Q factor (Q_E) or coupling (β) of the antenna by the relations:

$$Q_E \propto \omega_0 \frac{1}{|S_{21}|^2}$$

$$\beta \propto \frac{1}{\sqrt{\omega_0}} |S_{21}|^2$$

The response of the antenna is a typical high pass filter because there is a capacitive coupling with the field in the structure. In particular, by reducing the distance between the plate of the antenna and the strip of the coil, the cut-off frequency shift down, i.e. the antenna is able to damp also the resonant modes with low resonant frequencies (Figure 15 (a)).

If, instead, we increase the plate area, there is an initial increase of the coupling until the capacity between the plate and the vacuum chamber (C_2) short circuits the antenna (Figure 15 (b)) decreasing the coupling factor.

By considering the coupling of the antenna with the deflecting field of the kicker, we note that the antenna is a derivative circuit: the voltage on the adapted load Z_0 is the derivative of the voltage at point A in Figure 14.

With the simple models of Figure 16 it is possible to calculate the perturbation that the antenna introduces in the coil current and the amplitude of the ringing voltage on the adapted load Z_0.

Considering the ideal component we obtain the results shown of Figure 17. The perturbation in the current is practically negligible.

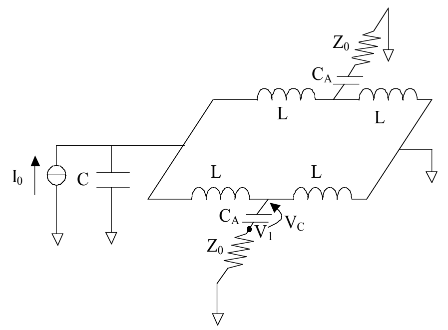

Figure 16: equivalent circuit to study the coupling between the antenna and the kicker pulse.

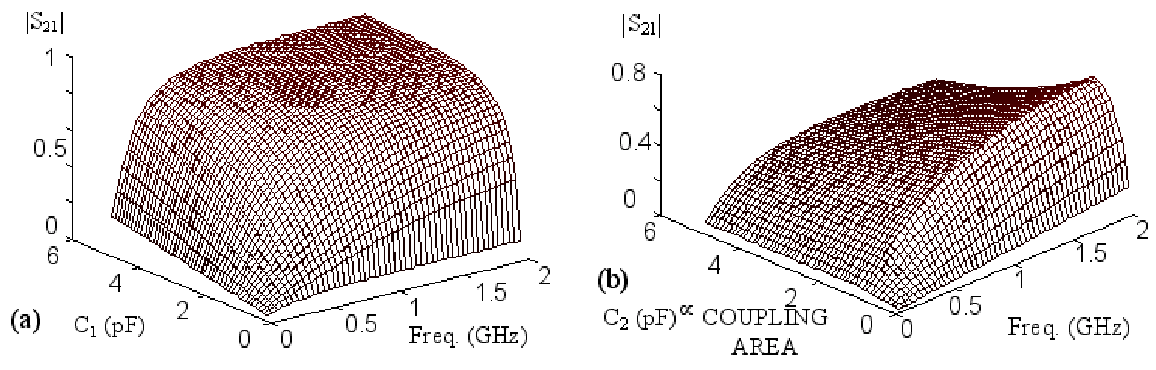

Figure 15: $|S_{21}|$ in the circuit of Figure 16 versus the plate dimension of the antenna.

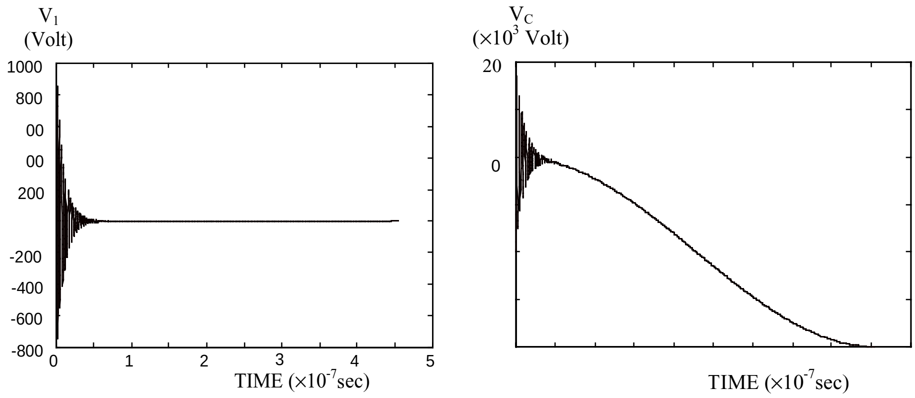

Figure 17: voltage behaviors in the circuit of Figure 16.

3.2 HFSS Simulations

By simulating the structure with the two antennas we obtain the results shown in Figs. 18-19 for the longitudinal and transverse cases respectively. We considered an antenna with the dimensions shown in Figure 20.

We note that in the structure with the antenna there is a reduction of the resonance Qs by a factor larger than 10 and, as the ratio R/Q with or without the antennas is constant, there is a correspondent reduction of the longitudinal and transverse impedance.

In the Q_E values there is an oscillation due to the fact that there are two contributions to the excitation of the antenna: a primary excitation on the plate of the antenna and a secondary one distributed along the strip of the antenna whose phase rotates with frequency with respect to the primary excitation.

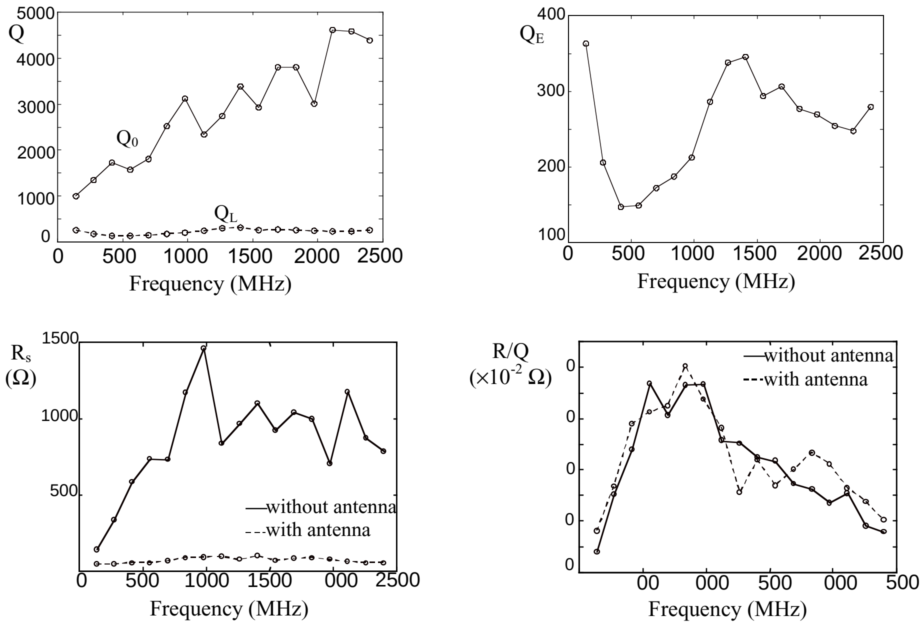

Figure 18: results obtained in the longitudinal case by HFSS.

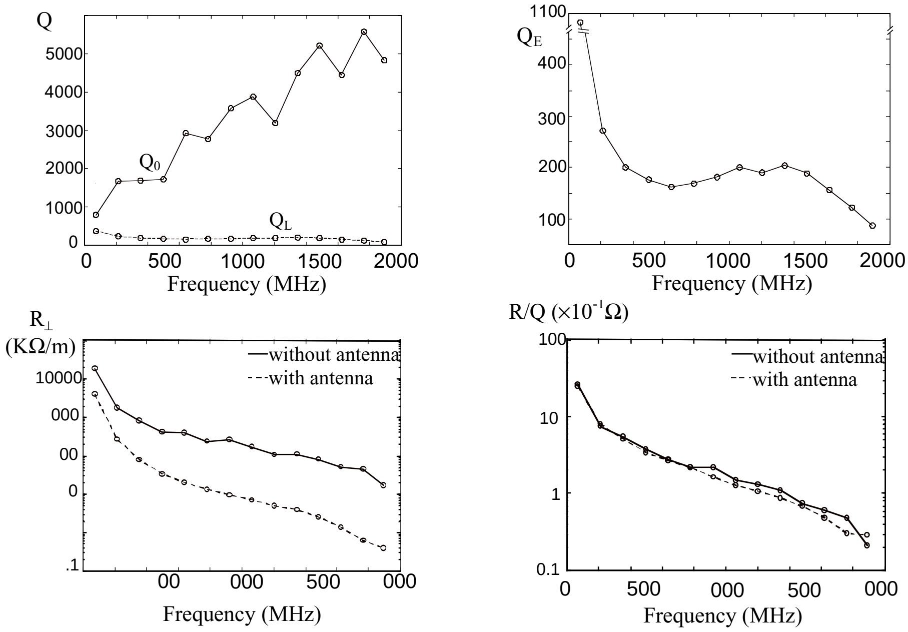

Figure 19: results obtained in the transverse case by HFSS.

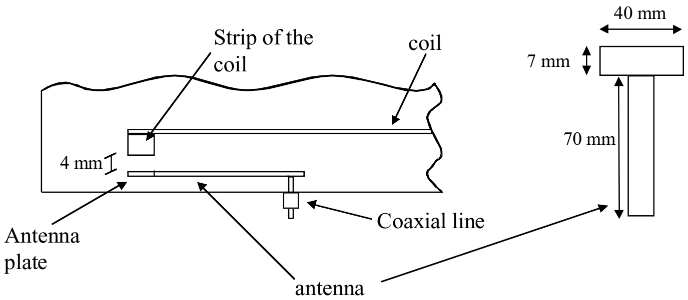

Figure 20: dimensions of the antenna used in the HFSS simulations

.

4 MEASUREMENTS ON THE PROTOTYPE WITH ANTENNAS

4.1 Wire measurements

The results of the measurements made on a prototype with the two antennas are shown in Figure 21-22 where the effect of capacitive coupling and the high pass response of the antennas are evident.

A comparison between the simulations results and the measurements is shown in Tables 5-6.

The external quality factors (Q_E) are in good agreement while the values of the ratio R/Q agree much better in the transverse case than in the longitudinal one due to the already mentioned critical dependence of the simulation results on the frequency accuracy (Figures 23–24).

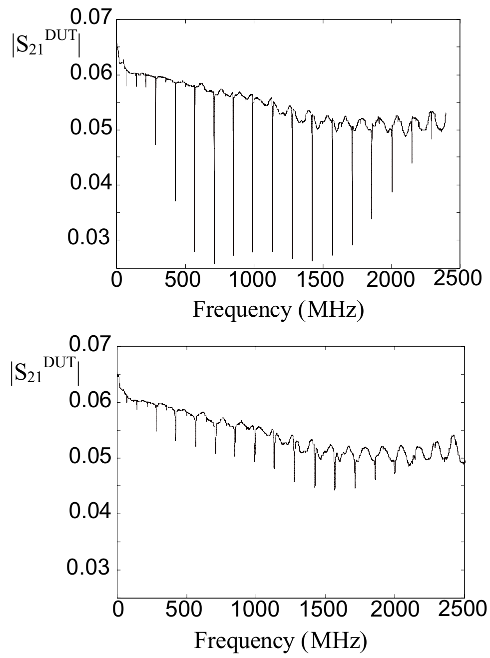

Figure 21: $|S_{21}|^{DUT}$ obtained by the measure of the longitudinal impedance with and without the antennas.

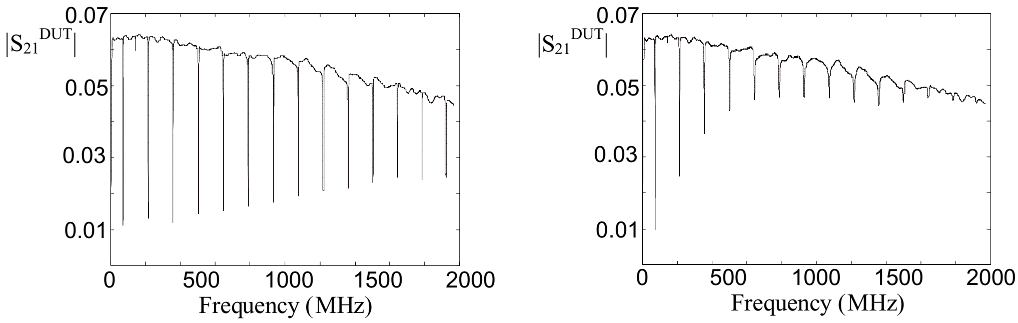

Figure 22: $|S_{21}|^{DUT}$ obtained by the measure of the vertical impedance with and without the antennas.

Table 5: Complessive results obtained by the measurements and by HFSS (longitudinal case).

LONGITUDINAL CASE

WIRE MEASUREMENTS									HFSS SIMULATIONS							
Without antenna				with antenna			Coupling Param.		without antenna			with antenna			Coupling Param.	
Res. Freq. (MHz)	Q_0	Rs_0 (Ω)	Rs_0/Q_0 ($\times 10^{-2}$)	Q_l	Rs_l (Ω)	Rs_l/Q_l ($\times 10^{-2}$)	Q_e	β	Q_0	R_{s0} (Ω)	R_{s0}/Q_0 ($\times 10^{-2}$)	Q_L	R_{sL} (Ω)	R_{sL}/Q_0 ($\times 10^{-1}$)	Q_e	β
142.4	854	20.5	**2.41**	251	16.5	**6.57**	**355**	2.4	1009	142	**14.07**	267	48	**17.98**	**363**	2.78
283.3	1113	108.9	**9.78**	180	34.5	**19.17**	**215**	5.18	1346	338	**25.11**	179	48	**26.82**	**206**	6.53
426.1	1579	266.1	**16.85**	148	41.0	**27.70**	**163**	9.69	1724	585	**33.93**	136	53	**38.97**	**148**	11.65
568.9	1886	420.6	**22.30**	139	43.8	**31.51**	**150**	12.57	1567	735	**46.90**	136	56	**41.18**	**149**	10.52
710.8	1776	469.2	**26.42**	137	45.5	**33.21**	**148**	12.00	1806	732	**40.53**	158	67	**42.41**	**173**	10.44
851.7	1509	447.6	**29.66**	156	47.7	**30.58**	**174**	8.67	2520	1171	**46.47**	175	88	**50.29**	**188**	13.40
992.8	1351	408.5	**30.24**	163	54.0	**33.13**	**185**	7.30	3124	1459	**46.70**	206	90	**43.69**	**213**	14.21
1135.2	1387	404.8	**29.18**	205	60.6	**29.56**	**241**	5.75	2339	835	**35.70**	255	97	**38.04**	**286**	8.18
1279.5	1572	412.2	**26.22**	237	71.2	**30.04**	**279**	5.63	2745	966	**35.19**	301	77	**25.58**	**338**	8.12
1425.2	1832	408.3	**22.29**	294	71.5	**24.32**	**350**	5.23	3386	1099	**32.46**	314	100	**31.85**	**346**	9.79
1570.7	1946	343.7	**17.66**	309	65.1	**21.07**	**367**	5.30	2920	924	**31.64**	267	72	**26.97**	**294**	9.93
1715.1	1915	266.8	**13.93**	314	52.0	**16.56**	**376**	5.09	3803	1040	**27.35**	283	85	**30.04**	**306**	12.43
1858.8	1839	190.9	**10.38**	278	37.0	**13.31**	**328**	5.61	3801	995	**26.18**	258	86	**33.33**	**277**	13.72
2002.6	1800	120.1	**6.67**	265	25.2	**9.51**	**311**	5.79	3002	707	**23.55**	248	77	**31.05**	**270**	11.12
2147.1	1812	75.0	**4.14**	305	12.3	**4.03**	**367**	4.94	4611	1173	**25.44**	242	64	**26.45**	**255**	18.08
2292.6	1868	42.5	**2.27**	340	8	**2.35**	**416**	4.49	4587	874	**19.05**	235	56	**23.83**	**248**	18.50

Table 6: complessive results obtained by the measurements and by HFSS (transverse case).

TRANSVERSE CASE

WIRE MEASUREMENTS											HFSS SIMULATIONS									
Without antenna					with antenna				Coupling Param.		without antenna				with antenna				Coupling Param.	
Res. Freq. (MHz)	Q_0	Rs_1 (Ω)	$Rs_{\perp 0}$ (KΩ/m)	Rs_1/Q_o ($\times 10^{-1}$)	Q_l	Rs_l (Ω)	$Rs_{\perp l}$ (KΩ/m)	Rs_l/Q_l ($\times 10^{-1}$)	Q_e	β	Q_0	Rs_1 (Ω)	$Rs_{\perp 0}$ (KΩ/m)	Rs_1/Q_o ($\times 10^{-1}$)	Q_l	Rs_1 (Ω)	$Rs_{\perp 0}$ (KΩ/m)	Rs_1/Q_o ($\times 10^{-1}$)	Q_e	β
71.7	597	1778	5258	**29.8**	420	1300	3858	**30.9**	**1416**	0.42	750	1876	8080	**25.0**	450	1101	4758	**24.4**	**1125**	0.92
215.2	765	843	831	**11.0**	250	264	261.7	**10.5**	**371**	2.06	1670	1243	1782.7	**7.44**	234	189	271.9	**8.08**	**272**	6.14
358.6	1110	735	435	**6.62**	185	115	68.25	**6.20**	**222**	5.00	1693	932	801.34	**5.51**	180	90.3	77.81	**5.02**	**201**	8.42
502.2	1279	608	257	**4.75**	160	69.8	29.62	**4.36**	**183**	6.99	1722	652	399.65	**3.79**	160	54.0	33.22	**3.38**	**176**	9.78
645.8	1392	501	164	**3.60**	149	48.5	15.99	**3.25**	**167**	8.34	2920	813	389.23	**2.78**	154	41.1	19.66	**2.67**	**163**	17.91
789.4	1516	435	117	**2.87**	139	40.7	10.97	**2.93**	**153**	9.91	2772	618	241.90	**2.23**	159	34.5	13.49	**2.17**	**169**	16.40
932.7	1571	375	85.2	**2.38**	149	34.7	7.913	**2.33**	**165**	9.52	3581	778	257.49	**2.17**	173	28.4	9.40	**1.64**	**182**	19.68
1075.8	1621	312	61.4	**1.92**	164	31.3	6.185	**1.91**	**182**	8.91	3872	577	165.76	**1.49**	191	24.2	6.97	**1.27**	**201**	19.26
1218.7	1667	270	47.1	**1.62**	162	30.9	5.387	**1.91**	**179**	9.31	3189	419	106.12	**1.31**	179	19.2	4.87	**1.07**	**190**	16.78
1361.4	1664	232	36.2	**1.39**	180	27.6	4.309	**1.53**	**202**	8.24	4500	491	111.44	**1.09**	195	17.0	3.85	**0.87**	**204**	22.06
1503.8	1739	197	27.8	**1.13**	187	21.7	3.066	**1.16**	**209**	8.32	5213	391	80.47	**0.75**	182	12.3	2.52	**0.68**	**189**	27.58
1645.7	1858	185	23.8	**0.99**	176	16.3	2.104	**0.93**	**194**	9.58	4444	272	51.22	**0.61**	152	7.29	1.37	**0.48**	**157**	28.31
1786.0	1826	169	20.0	**0.92**	163	11.0	1.307	**0.68**	**179**	10.20	5577	267	46.30	**0.48**	120	3.55	0.61	**0.30**	**123**	45.34
1921.8	1824	146	16.1	**0.80**	142	5.5	0.607	**0.39**	**154**	11.84	4838	104	16.74	**0.21**	85	2.49	0.40	**0.29**	**87**	55.61

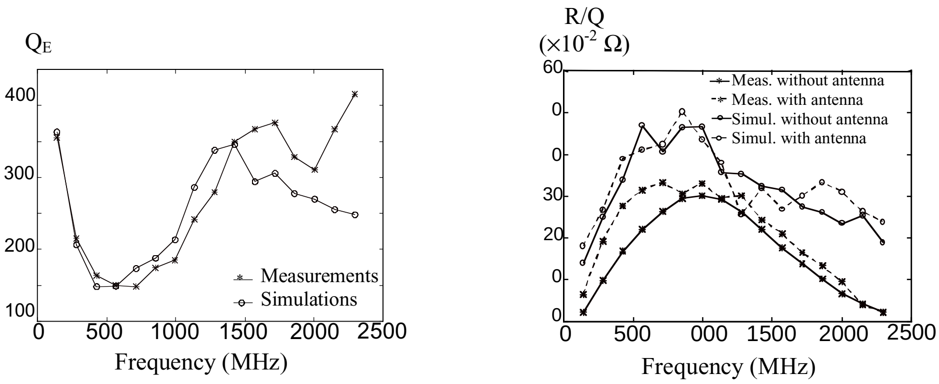

Figure 23: Q_E and R/Q obtained by HFSS and by the measurements in the longitudinal case

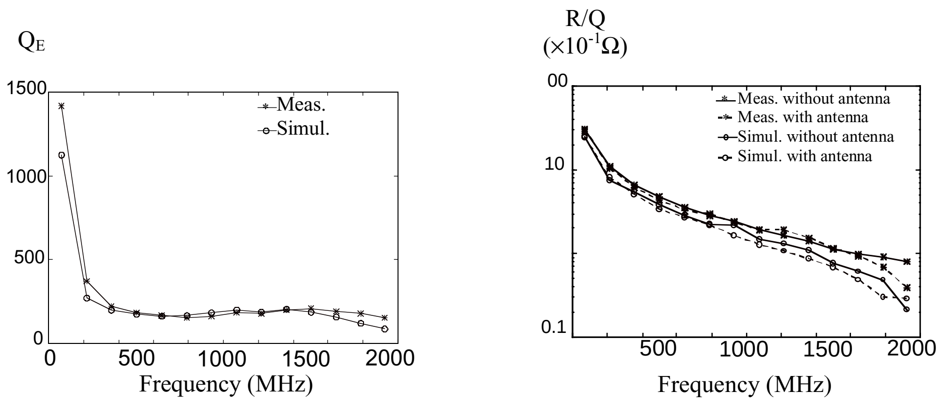

Figure 24: Q_E and R/Q obtained by HFSS and by the measurements in the vertical case.

4.2 Q Measurements

By measuring the transmission scattering parameter $S_{antenna1-antenna2}$ it is possible to calculate the coupling parameters (Q_E, β) between the antennas and the cavity. This measurement confirms the results obtained with the wire method as it is evident from Tabs. 7-8 where the results obtained by modifying the distance between the antennas and the strips of the coils are also reported. In particular, reducing the distance, the antenna became more efficient in damping the resonant modes with low resonant frequencies.

Table 7: Q measurements compared with wire measurements (longitudinal case).

LONGITUDINAL CASE

Q meas.						wire meas.						Q meas. versus distance antenna-strips					
without antenna		with antenna		coupl. param.		Without antenna		With antenna		Coupl. Param.		Distance: 2.5 mm			Distance: 5.5 mm		
Res. Freq. (MHz)	Q_0	Res. Freq. (MHz)	Q_l	Q_e	β	Res. Freq. (MHz)	Q_0	Res. Freq. (MHz)	Q_l	Q_e	β	Q_l	Q_e	β	Q_l	Q_e	β
142.2	861	140.9	235	**323**	2.67	142.4	854	141.1	251	**355**	2.40	119	**138**	6.24	322	**514**	1.68
282.5	1293	280.2	151	**171**	7.56	283.3	1113	281.1	180	**215**	5.18	68	**72**	17.96	231	**281**	4.60
424.9	1896	421.9	148	**160**	11.85	426.1	1579	423.1	148	**163**	9.69	60	**62**	30.58	230	**262**	7.24
567.4	2123	564.0	145	**156**	13.61	568.9	1886	565.6	139	**150**	12.57	57	**59**	35.98	240	**271**	7.83
709.1	1980	705.5	143	**154**	12.86	710.8	1776	707.4	137	**148**	12.00	52	**53**	37.36	262	**302**	6.56
849.9	1441	846.2	147	**164**	8.79	851.7	1509	848.4	156	**174**	8.67	52	**54**	26.69	292	**366**	3.94
990.8	1209	987.2	205	**247**	4.89	992.8	1351	989.8	163	**185**	7.30	64	**68**	17.78	402	**602**	2.01
1133.4	1338	1129.7	242	**295**	4.54	1135.2	1387	1132.7	205	**241**	5.75	71	**75**	17.84	492	**778**	1.72
1277.7	1684	1274.1	299	**363**	4.64	1279.5	1572	1277.1	237	**279**	5.63	86	**91**	18.51	614	**966**	1.74
1423.5	2107	1420.0	343	**410**	5.14	1425.2	1832	1422.8	294	**350**	5.23	102	**107**	19.69	744	**1150**	1.83
1569.1	2147	1565.4	361	**434**	4.95	1570.7	1946	1568.0	309	**367**	5.30	116	**123**	17.46	757	**1169**	1.84
1713.6	2065	1709.6	406	**505**	4.09	1715.1	1915	1712.3	314	**376**	5.09	124	**132**	15.64	751	**1180**	1.75
1857.2	1938	1853.1	403	**509**	3.81	1858.8	1839	1855.4	278	**328**	5.61	141	**152**	12.75	674	**1033**	1.88
2001.1	1891	1997.0	278	**326**	5.80	2002.6	1800	1999.3	265	**311**	5.79	163	**178**	10.62	539	**754**	2.51

Table. 8: Q measurements compared with wire measurements (transverse case).

TRANSVERSE CASE

Q meas.						wire meas.						Q meas. versus distance antenna-strips					
without antenna		with antenna		Coupl. Param.		Without antenna		With Antenna		Coupl. Param.		Distance: 2.5 mm			Distance: 5.5 mm		
Res. Freq. (MHz)	Q_0	Res. Freq. (MHz)	Q_l	Q_e	β	Res. Freq. (MHz)	Q_0	Res. Freq. (MHz)	Q_l	Q_e	β	Q_l	Q_e	β	Q_l	Q_e	β
71.3	641	71.5	430	**1305**	0.49	71.7	597	71.5	420	**1416**	0.42	350	**771**	0.83	520	**2755**	0.23
215.5	937	214.0	273	**385**	2.43	215.2	765	213.8	250	**371**	2.06	112	**127**	7.38	358	**579**	1.62
359.2	1172	356.9	175	**206**	5.69	358.6	1110	356.7	185	**222**	5.00	74	**79**	14.84	271	**352**	3.32
503.0	1288	500.0	160	**183**	7.04	502.2	1279	499.8	160	**183**	6.99	62	**65**	19.82	261	**327**	3.93
646.8	1418	643.4	165	**187**	7.58	645.8	1392	643.2	149	**167**	8.34	59	**62**	22.87	280	**349**	4.06
790.6	1558	786.9	151	**167**	9.33	789.4	1516	786.7	139	**153**	9.91	53	**55**	28.33	280	**341**	4.56
934.2	1601	930.2	150	**166**	9.64	932.7	1571	929.9	149	**165**	9.52	51	**53**	30.21	308	**381**	4.20
1077.5	1581	1073.6	173	**194**	8.15	1075.8	1621	1073.2	164	**182**	8.91	56	**58**	27.26	364	**473**	3.34
1215.6	1510	1216.9	208	**241**	6.27	1218.7	1667	1216.3	162	**179**	9.31	63	**66**	22.88	433	**607**	2.49
1363.4	1750	1359.7	207	**235**	7.45	1361.4	1664	1358.3	180	**202**	8.24	65	**68**	25.74	438	**584**	3.00
1505.6	1737	1502.2	219	**251**	6.92	1503.8	1739	1500.9	187	**209**	8.32	73	**76**	22.86	458	**622**	2.79
1647.2	1795	1644.0	170	**188**	9.55	1645.7	1858	1642.6	176	**194**	9.58	70	**73**	24.59	386	**492**	3.65
1787.3	1802	1784.3	174	**193**	9.34	1786.0	1826	1783.5	163	**179**	10.20	73	**76**	23.71	365	**458**	3.94
1922.7	1381	1920.6	124	**136**	10.15	1921.8	1824	1920.6	142	**154**	11.84	67	**70**	19.73	240	**290**	4.75

4.3 High voltage tests

Figure 25 shows the voltage signal output from the antenna during the kicker pulse in a test made on a prototype.

As already mentioned the antenna is a derivative circuit and the perturbation of the current in the two coils with or without the antenna is negligible.

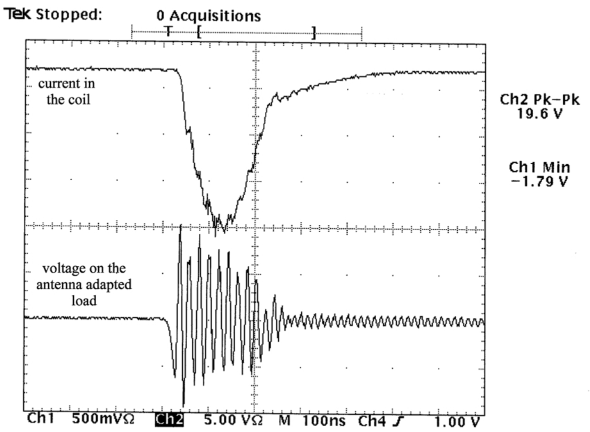

Figure 25: voltage on the antenna adapted load and current in the coils measured during the kicker pulse.

5 CONCLUSIONS

In this work we propose a solution to damp the resonant modes in the DAΦNE injection kickers that, from experimental observation, are responsible for multibunch instabilities.

To study the different resonant modes in the structure we introduced a simple model of the kicker based on the multiconductor transmission lines theory. This analysis allowed us to understand how the fields interact with the beam and to calculate the longitudinal and transverse impedance of the structure.

From the knowledge of the field configuration in the structure an effective antenna has been designed.

With a simple model we verified, also, that the antenna does not perturb the kicker deflecting field and measurements on a prototype equipped with two antennas confirmed the effectiveness of the solution in strongly reducing the kicker longitudinal and vertical coupling impedances.

To summarize, the solution presents the following advantages:

a) it is possible to modify the existing kickers without modification of the pulse generation system;

b) the deflecting field is not significantly perturbed by the antennas;

c) the antennas are able to damp the longitudinal and transverse modes.

It is also possible an insertion of a ceramic material between the connection strips and the antenna plate to increase the coupling capacitance, i.e. to shift the cut off frequency of the antenna towards the low frequencies.

REFERENCES

[1] S. De Simone, A. Drago and A. Ghigo, “Accumulator Kicker Magnetic Measurements”, DAFNE Technical note MM-2, Frascati, 1993.

[2] S. De Simone and A. Ghigo, “DAFNE Accumulators Kickers”, 3th European Particle Accelerator Conferance Proceedings, Berlin, 24-28 March 1992 p.1449.

[3] M. Sands and J. Rees, “A Bench Measurement of the Energy Loss of a Stored Beam to a Cavity”, SLAC-Report PEP-95, August 1974.

[4] F. Caspers, “Beam Impedance Measurements Using the Coaxial Wire Method”, Proc. Of the Workshop on Impedance and Current Limitations, ESRF-Grenoble, CERN PS/88-59, October 1988.

[5] A. Argan, “L’impedenza Longitudinale negli Acceleratori di Particelle”, Tesi di Laurea A.A. 1996-97, Napoli.

[6] A. Argan, L. Palumbo, M.R. Masullo, V.G. Vaccaro, “On The Sands And Rees Measurement Method of the Longitudinal Coupling Impedance”, Particle Accelerator Conference, New York, 1999, Proceeding in stampa.

[7] H. Hahn and F. Pedersen, “On Coaxial Wire Measurement of the Longitudinal Coupling Impedance”, BNL 50870, Particle Accelerators and High-Voltage Machines TID-4500, April 1978.

[8] L. Palumbo, V. G. Vaccaro, ”Wake Fields Measurements”, LNF-89/035 (P), Frascati, 1989.

[9] Hewlett Packard, “HP 85180A High-Frequency Structure Simulator. User’s Reference. Release 4.0”, Hewlett Packard, 1996.